Surface coatings to mitigate phase separation in LiFePO4 during lithium-ion battery discharge

Matter

Article

Surface coatings to mitigate phase separation in $LiFePO_4$ during lithium-ion battery discharge

Graphical abstract

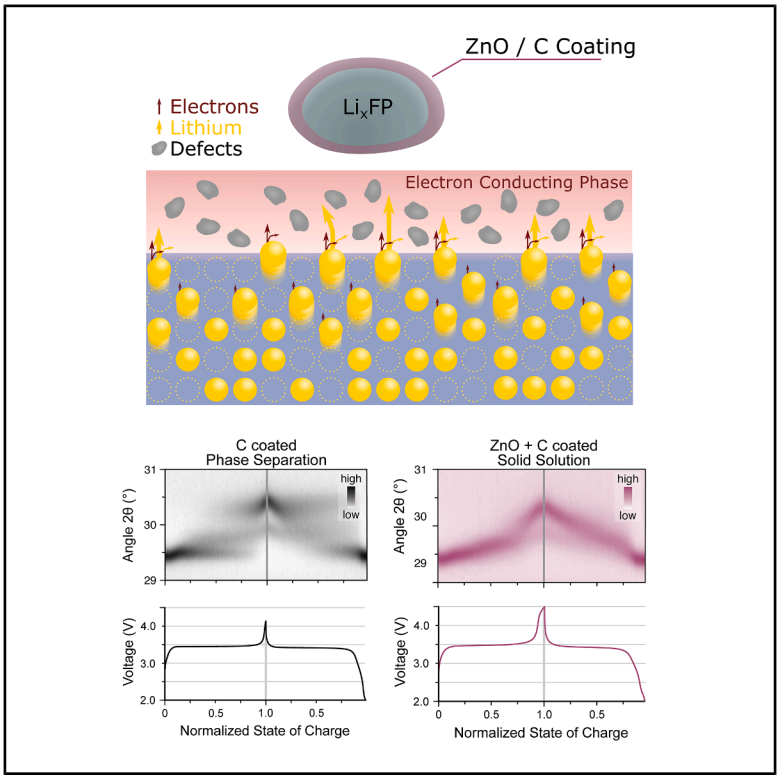

Authors

Peter Benedek, Xueyan Zhao, Emanuel Rudolf Bileter, ..., Fanni Juranyi, Martin Månsson, Vanessa Claire Wood

Correspondence

vwood@ethz.ch

In brief

This work addresses a battery failure mechanism where active material particles are strained internally by separating into Li-rich and Li-poor regions during cycling. We demonstrate that these intrinsic inhomogeneities can be prevented by engineering a surface coating that controls the movement of lithium ions at the particle interface. This new understanding is used to create a mixed ceramic-carbon-coated material that delivers excellent phase uniformity and fast charging capability.

Highlights

- A novel, transferable method characterizes surface charge dynamics
- Coatings kinetically control phase separation in battery active materials
- Engineered coating inhibits $LiFePO_4$ phase separation while maintaining rate capability

3 Understanding
Dependency and conditional studies on material behavior

Benedek et al., 2026, Matter 9, 102725
June 3, 2026
https://doi.org/10.1016/j.matt.2026.102725

CellPress

Matter

CellPress
OPEN ACCESS

Article

Surface coatings to mitigate phase separation in $LiFePO_4$ during lithium-ion battery discharge

Peter Benedek,[1,7,8,10] Xueyan Zhao,[1,10] Emanuel Rudolf Bileter,[2] Annina Moser,[1] Ola Kenji Forslund,[3] Nami Matsubara,[3] Elisabetta Nocerino,[3] Stephen Cottrell,[4] Marisa Medarde,[5] Yasmine Sassa,[6] Ramesh Shunmugasundaram,[1] Thomas Francisco Jaramillo,[7,8] Andreas Borgschulte,[2] Fanni Juranyi,[9] Martin Månsson,[3] and Vanessa Claire Wood[1,11,*]

[1]Department of Information Technology and Electrical Engineering, ETH Zurich, 8092 Zurich, Switzerland
[2]Laboratory for Advanced Analytical Technologies, Empa - Swiss Federal Laboratories for Material Science and Technology, 8600 Dübendorf, Switzerland
[3]Department of Applied Physics, KTH Royal Institute of Technology, 16440 Stockholm, Sweden
[4]ISIS Neutron and Muon Facility, Rutherford Appleton Laboratory, Didcot, Oxfordshire OX11 0QX, UK
[5]Laboratory for Multiscale Materials Experiments, Paul Scherrer Institute, 5232 Villigen PSI, Switzerland
[6]Department of Physics, Chalmers University of Technology, 41296 Gothenburg, Sweden
[7]SUNCAT Center for Interface Science and Catalysis, SLAC National Accelerator Laboratories, Menlo Park, CA 94025, USA
[8]Department of Chemical Engineering, Stanford University, Stanford, CA 94043, USA
[9]Laboratory for Neutron Scattering and Imaging, Paul Scherrer Institute, 5232 Villigen, Switzerland
[10]These authors contributed equally
[11]Lead contact
*Correspondence: vwood@ethz.ch
https://doi.org/10.1016/j.matt.2026.102725

PROGRESS AND POTENTIAL The stability and long-term performance of lithium-ion batteries are fundamentally limited by inhomogeneous electronic and ionic transport. While efforts often focus on microscale uniformity (e.g., electrode fabrication), nanoscale homogeneity is equally crucial. A key challenge is the unequal distribution of Li ions within active materials, which drives non-uniform local current density. For many insertion materials (e.g., $LiFePO_4$), this results in phase separation, causing local current hotspots and forming new phase boundaries. This decomposition is detrimental to electrode performance, leading to extra stresses, loss of rate capability, and accelerated aging. Significant research has established that phase separation is linked to the Li dynamics at the particle surface and within the bulk. In this study, we use $LiFePO_4$ as a model system to demonstrate that phase separation can be actively controlled by engineering the particle's surface coatings. We verify this physical mechanism through systematic experiments and *ab initio* calculations on $LiFePO_4$ particles with different coatings. We successfully applied these findings to create a mixed ceramic-carbon coating capable of simultaneously stabilizing phase integrity during slow cycling (C/10) while maintaining superior high-rate performance (5C).

SUMMARY

To achieve long-lasting, high-performance lithium-ion batteries, local inhomogeneity in current density must be avoided. One driver of such inhomogeneity is the spinodal decomposition of active materials into Li-rich and Li-poor phases during charge and discharge, respectively. Whether or not such phase separation occurs is linked to the dynamics of lithium (Li) at the active material surface and within its bulk. Here, we show that particle surface coatings can be designed to inhibit phase separation. Using $LiFePO_4$ as a model system, we prepare particles with different coatings in order to tune Li dynamics and electronic structure and thereby induce or prevent phase separation, which we verify through experiment and *ab initio* calculations. We then leverage our findings to create a mixed ceramic-carbon coating that mitigates phase separation down to rates as low as 0.1C and simultaneously enables fast (dis)charge up to 5C.

INTRODUCTION

To be able to store energy in lithium-ion batteries (LIBs) reversibly over thousands of cycles, homogeneous transport of electrons and lithium (Li) throughout the entire cell is crucial. To achieve such an evenly distributed current density in a complete cell, LIBs consist of complex, hierarchical structures containing electrochemically active materials, ion conducting electrolytes,

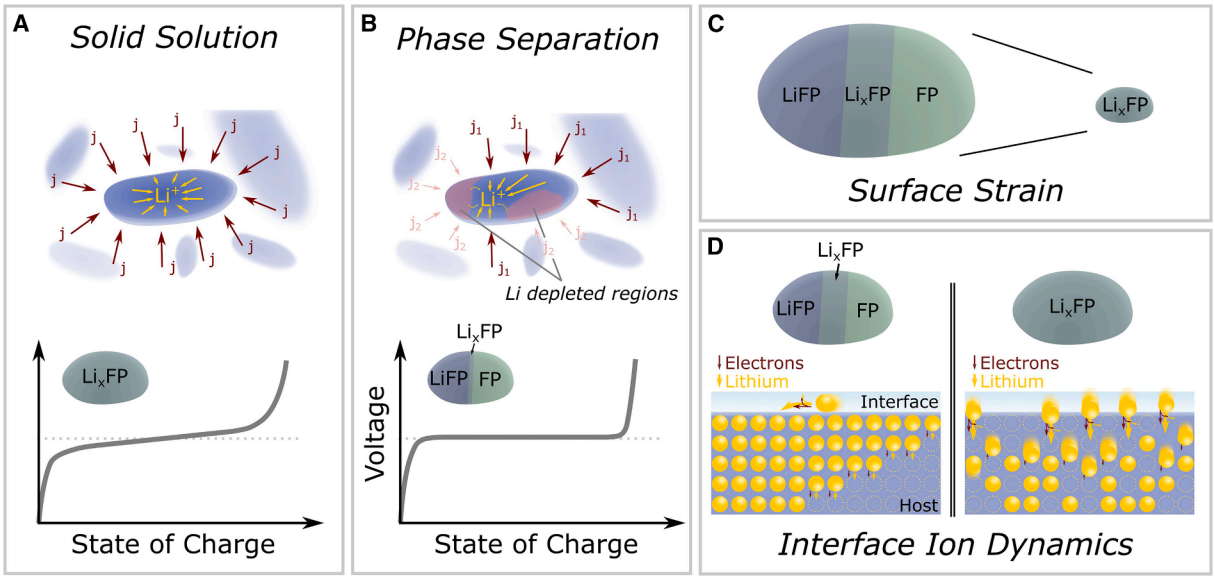

Figure 1. Understanding parameters that govern solid solution vs. phase separation in battery active materials

Comparison of the local current density in the vicinity of the active particles (top) and the resulting voltage polarization (bottom) in the case of (A) solid solution behavior and (B) phase separation. Strategies to mitigate phase separation include (C) reducing the particle size and (D) changing charge dynamics at the particle interface. When the surface charge diffusion is faster than the charge transfer, lithium ion phase separate into Li-rich and Li-poor regions. Conversely, a reduction of the surface charge diffusion facilitates solid solution behavior.

and electron conducting carbon black-binder.[1] While optimization of the slurry mixing and electrode fabrication is used to achieve uniformity on the microscale, maintaining uniformity on the nanoscale requires engineering of the active particles and their interfaces to the electric and ionic networks.[2–6] One challenge is the change of the Li concentration within the active materials which influences the chemical potential and intercalation dynamics.[7] While many insertion materials (e.g., layered transition metal oxides) maintain a single solid solution phase over a wide Li concentration range (Figure 1A), numerous insertion materials (e.g., $LiFePO_4$) can suffer from a spinodal decomposition into Li-rich and Li-poor phases, which is seen as a characteristic plateau in voltage vs. capacity plots during (dis)charge (Figure 1B). This can cause a non-uniform current distribution in and around the active particles. The resulting local current hotspots and new phase boundaries give rise to stresses and overpotentials, leading to loss of (dis)charging rate capability,[8,9] and cell aging.[10–12]

Significant work has been conducted during the last decades to understand and solve phase separation on a single particle level in $LiFePO_4$ (LFP) that exhibits a single, two-phase decomposition into $LiFePO_4$ and $FePO_4$ domains. Three key phenomena have been identified. First, when the primary particle size decreases below the characteristic phase boundary size (~50 nm[13–15]), strain between the two phases hinders formation of multiple phases within a single particle such that a solid solution is favored (Figure 1C).[16] Second, phase separation is affected by the (dis)charging rate. For rates above 5C, a solid solution can be maintained over a larger state-of-charge window,[17–19] particularly during lithiation.[2,7,9] Third, particles with a solid solution Li_xFePO_4 left at open circuit potentials in electrolyte revert to phase-separated $LiFePO_4$ and $FePO_4$ due to an electrolyte-mediated surface diffusion mechanism.[19,20]

The theoretical framework developed by Nadkarni et al.[9] and confirmed by Li et al.[2,20] explains these findings through the exchange current densities and charge transfer overpotentials that change as a function of lithiation and which lead to auto-catalysis or -inhibition of spinodal decomposition.[7,8] In a simplified picture,[21] two scenarios emerge during the auto-inhibited lithiation (Figure 1D): (1) when the charge transfer reaction rate is small, Li ions move at the particle surface to form Li-rich and Li-poor regions such that the exchange current density remains constant and phase separation occurs. (2) At charge transfer reaction rates faster than the surface diffusion, lithium intercalates directly into Li_xFePO_4 and solid solution formation is favored. Therefore, the critical current, which delineates the regimes where lithiation occurs via spinodal decomposition or via solid solution, is determined by the Li and electron surface diffusivities and the charge transfer reaction rate. However, due to the lack of understanding of how charge transport occurs at the surface of Li ion battery materials, particularly those coated with ceramics[22,23] or carbon,[24] reduction of the critical current has been achieved by experimental trial and error.

Here, we computationally and experimentally study interfacial charge dynamics in order to rationally design and demonstrate a coating that reduces the critical current, therefore enabling lithiation via a solid solution mechanism over a broad range of discharge rates. We synthesize $LiFePO_4$ particles with different surface coatings in order to experimentally study the lithium ion dynamics at the surface of $LiFePO_4$ and its impact on the lithiation mechanism. We gain further insight into our experimental findings via density functional theory (DFT) and *ab initio*

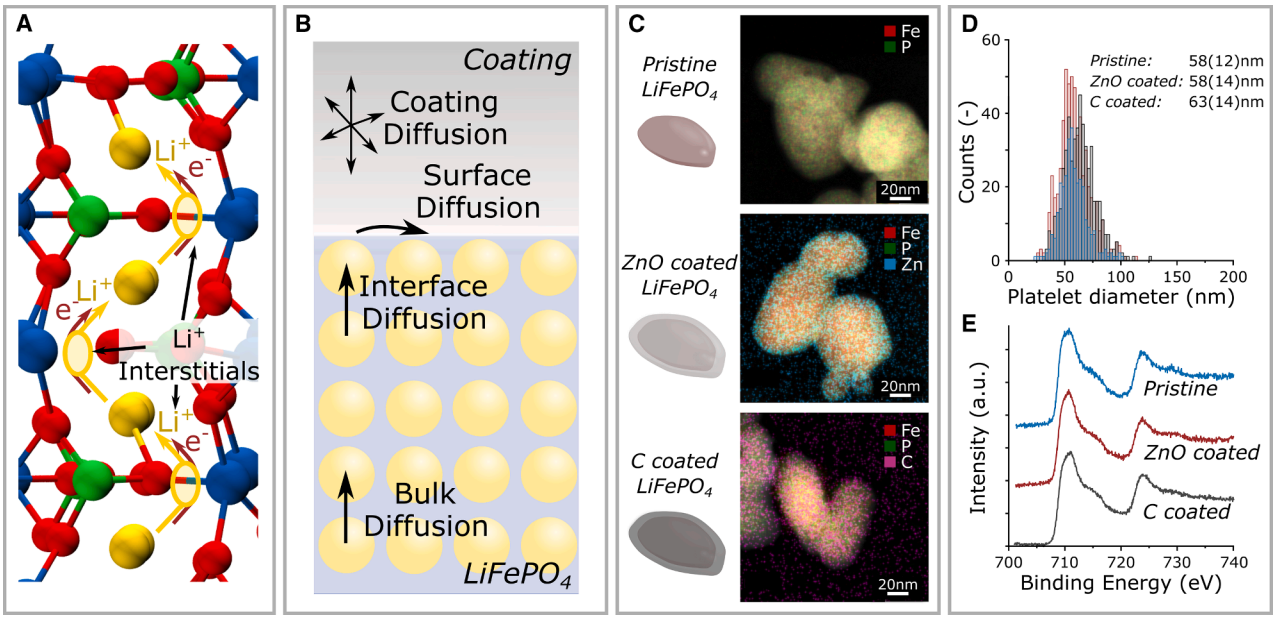

Figure 2. Ion transport in $LiFePO_4$ and characterization of the coated $LiFePO_4$ particles used in this study

(A) In bulk $LiFePO_4$, Li ions and electrons move collectively along the lattice via one interstitial Li-ion site.

(B) Schematic of the four different diffusion pathways to be considered in coated $LiFePO_4$ particles.

(C) Energy dispersive X-ray scattering scanning transmission electron microscopy (STEM-EDX) image of the pristine, ZnO-, and carbon-coated $LiFePO_4$ nanoparticles.

(D) Particle size dispersion of the three samples.

(E) X-ray photoemission spectra of the three samples, displayed at the Fe L edge.

molecular dynamics calculations of surface electronics and ionics. Based on these findings, we propose and demonstrate a coating that enables solid solution Li_xFePO_4 at cycling rates as low as C/10 while also maintaining the rate capability and (dis)charge capacity. This work highlights how coatings can be used to control charge dynamics at interfaces and provides a rational approach to designing novel coatings to suppress phase separation in lithium-ion battery active materials.

RESULTS AND DISCUSSION

Rationale for the investigated system

Whether lithiation occurs via phase separation or solid solution will be determined by the rate at which lithium ions and electrons arrive at or leave a particle and the relative rates of bulk diffusion, interface diffusion, and surface diffusion for that particle (Figure 2B). Here, we use the term "interface diffusion" to refer to diffusion through the outermost layers of the LFP. We use the term "surface diffusion" to refer to diffusion occurring parallel to the LFP surface. For a coated particle, one must further consider the impact of charge motion in the coating. Ideally, we would be able to measure each diffusion rate; however, in practice, it is extremely challenging to experimentally differentiate bulk, interface, and surface diffusion.

Our selection of LFP as a model system simplifies some of the considerations for bulk diffusion significantly since it is well-established that Li diffusion occurs in 1D along the [010] direction. For the particle bulk, previous work has shown that the lithium ion and electron (obtained from oxidation of Fe from Fe^{2+} to Fe^{3+}) move collectively through the lattice via a small polaron hopping mechanism (Figure 2A).[25,26] The Li hopping to a neighboring site (separated by 3 Å) via an interstitial site at ~1.8 Å is activated by a multi-phonon process with an activation barrier of approximately 350 meV.[25,27,28]

More challenging is differentiating between surface and interface diffusion. We know that surface reconstruction affects the local LFP structure and vibrational motion at the surface,[29] and undercoordination of the LFP surface leads to a lower activation barrier of ~200 meV for Li interface diffusion.[30] In the case of surface diffusion, electrolyte molecules (or water) can shuttle Li ions from one site to another and carbon-coated particles accelerate this surface diffusion process.[20]

We therefore use LFP with different coatings in order to systematically distinguish between processes involving the particle bulk, interface layers, surface, and coatings. Specifically, we compare uncoated LFP, LFP with an electronically insulating ZnO coating, and LFP with a conductive C coating. Because Li concentrations in coatings are low,[31,32] differences in the experimental or computational findings on Li dynamics in the steady-state can be attributed to either surface or interface diffusion. The difference in the electronic properties of the conductive carbon and insulating ZnO allow us to study surface electronic effects.

We synthesize $LiFePO_4$ nanoparticles (Figure 2C) by a hydrothermal synthesis approach.[29,33] We work with particles ~60 nm in diameter (Figure 2D), which means that size should not

influence the occurrence of phase separation (size below which solid solutions occur is 50 nm[14–16]). An amorphous zinc oxide or carbon coating is obtained by annealing zinc(II) acetate or D-glucose, respectively, with the $LiFePO_4$ nanoparticles at 400°C–600°C.[23,31] Energy dispersive X-ray scattering scanning tunneling microscopy (Figure 2C) indicates an approximately 3–5-nm-thick amorphous coating (Figure S17). X-ray diffraction (Figure S18) and Fourier transform infrared spectroscopy (Figure S19) suggest that the bulk properties of the $LiFePO_4$ samples are unaffected by the coating. X-ray photoemission spectroscopy (XPS) show no change in the Fe2p energy states and that all surfaces are Fe^{2+} terminated,[34] confirming that the $LiFePO_4$ surface is unaffected by the coating (Figures 2E and S1). An elemental analysis using inductively coupled plasma mass spectrometry (see Table S3) suggests some variation in the stoichiometry of each sample, with a 2% lithium deficiency in the ZnO-coated sample. However, for the sake of simplicity, we assume stoichiometric $LiFePO_4$ surfaces.

Investigation of ion dynamics in $LiFePO_4$

To measure lithium-ion dynamics, we employ muon spin spectroscopy (μ^+SR), where one measures the spin relaxation behavior of a pulse of spin-polarized antimuons implanted into the sample.[35,36] We select μ^+SR for three reasons. First, as a resonance-based technique, μ^+SR can probe local motion of the Li ions. As a result, the absence of the Li ions in the coating layers allows us to neglect coating diffusion contributions. Second, the high gyromagnetic ratio of muons allows us to distinguish between paramagnetic Fe and dynamic Li contributions in $LiFePO_4$,[37] making it more suitable than more conventional Li nuclear magnetic resonance spectroscopy. Third, by systematically studying particles of same composition but different sizes and surface to volume ratios, we showed that μ^+SR can detect Li diffusion associated with the interface or surface of nanoparticles that have a high ratio of surface atoms contributing to a signal.[30]

Here, we fit the μ^+SR data over the investigated temperature range of 100–400 K (Note S2) and find that carbon-coated LFP particles show an Arrhenius-type behavior with an activation energy of 160(30) meV, which we associate with lithium ion hopping (Figure 3A). In contrast, the ZnO coated and pristine terminated samples exhibit no signal, which means that, similar to Li hoping in bulk LFP,[30] any Li hopping within or at the surface of the ZnO-coated LFP occurs with an activation energy above 350 meV (which would only be visible above 400 K).

We previously attributed the observation of diffusion with an activation energy of 160 meV in carbon-coated LFP nanoparticles to undercoordination of the outmost atomic layers and thus a lower energy barrier for Li hopping through the LFP interface region.[30] However, if undercoordination were the only reason for the reduced diffusion activation barrier, we would expect the uncoated, pristine LFP nanoparticles to also exhibit a low activation energy process, which they do not. Therefore, we conclude that the process we observe in the carbon-coated LFP nanoparticles is likely linked to improved Li surface diffusion at the LFP-carbon interface.

To investigate how the carbon and ZnO coatings could influence surface diffusion, we computationally study the electronic properties of the LFP particles with ZnO and carbon coatings and the Li diffusion. We perform DFT using the CP2k package that, as a hybrid plane wave and orbital-based method, offers the possibility to study local surface effects.[38–40] We construct and geometrically relax $LiFePO_4$ slabs with a thickness of 3.5 unit cells along the [010] direction with periodic boundary conditions perpendicular to the [010] direction to obtain quasi-infinite platelet particles (Figure 3A) with (1) a pristine $LiFePO_4$ (010) surface (Figure 3B), (2) an amorphous ZnO-coated $LiFePO_4$ (010) surface (Figure 3C), and (3) a covalently bonded, carbon-coated $LiFePO_4$ (010) surface (Figure 3D). We validate these calculations by comparing the calculated electronic structure to that determined by XPS and UV-visible absorption spectroscopy (Figures S1, S2, and S20).

We determine the elemental and positional origin of each electronic state (Figures S3–S5), allowing us to plot the partial electron density of states (PEDOS) within the slab (Figure 3B) and at the surfaces (Figures 3C–3E). In agreement with literature calculations and measurements,[41–44] the pristine LFP slab has a band gap of 3.6 eV within the slab with hybridized Fe–O valence band states and Fe conduction band states (Figure 3B). At the pristine surface (Figure 3C), the valence and conduction band states remain unchanged, suggesting only minor differences in electronic structure between surface and bulk. This is further supported when looking at the highest occupied and lowest unoccupied electronic states (inset of Figure 3C), where significant contributions to the electronic wave functions arise from deeper within the slab. When the (010) surface is terminated with ZnO (Figure 3D), electronic states stemming from ZnO are present within the LFP band gap. The carbon termination (Figure 3E) also results in mid-gap states. However, in contrast to the ZnO case where the mid-gap wave function states are strongly localized in the ZnO layer (inset Figure 3D), the carbon coating leads to a Fe-*O*-C hybridization with electronic density between the coating and the particle bulk (inset Figures 3E and S6). These results suggest that, while the ZnO coating will not significantly affect electronic or ionic transport at the LFP surface, the carbon coating will. Specifically, the delocalization of the electron could decrease the energy barrier for Li ion hopping dynamics, which is consistent with our findings from the μ^+SR measurements.

We confirm the enhanced Li ion dynamics computationally by performing ab initio molecular dynamics simulations (AIMD) on the $LiFePO_4$ slabs described previously at a cryostat temperature of 1000 K, where the thermal energy is high enough to observe lithium ion hopping without impacting the structural integrity of the slab[28,41,45] (Figure S7). First, we calculate the Li mean squared displacement (MSD) using the pinball model,[46] where all atoms are fixed to their 0 K equilibrium position except for the Li atoms (Figure S8), in order to study the motion of the Li atoms independent of the motion of other atoms in the lattice. In all samples, the Li ions exhibit small quasi-harmonic fluctuations at a frequency of approximately 5–15 THz, which corresponds to typical Li–O vibrations in $LiFePO_4$[29] (Figure S8); however, the amplitude of these vibrations varies significantly among the samples (Figure 3F). Within the slabs and at the surface of the ZnO-terminated and pristine samples, Li atoms fluctuate with an MSD of ~0.5 $Å^2$, (amplitude of ~0.7 Å). In contrast, in the carbon-coated samples, the MSD more than doubles to 1.1 $Å^2$

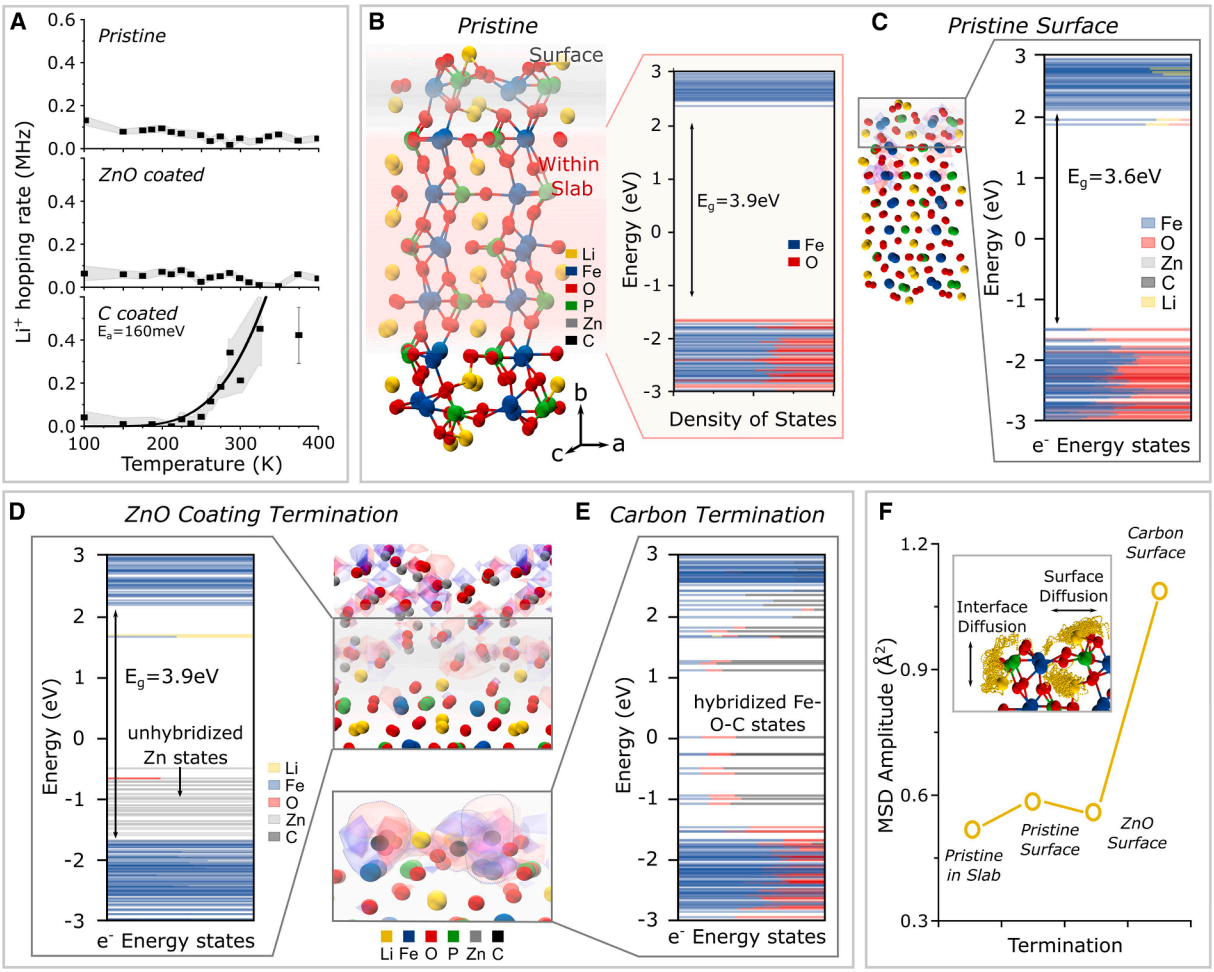

Figure 3. Density functional theory simulations to study electronic and ion transport in coated $LiFePO_4$

(A) Li-ion hopping rate of the coated $LiFePO_4$ (LFP) nanoparticle powders obtained from muon spin spectroscopy. On the carbon coated $LiFePO_4$, Li-ion dynamics show an activation energy of 160 meV. The shaded gray region indicates the uncertainty of the fitted activation barrier values, as obtained from the fitting procedure.

(B) Structure of the LFP slabs with a classification between atoms at the surface and within the slab. Furthermore, the partial electron density of states (PEDOS) is shown for the pristine LFP sample within the slab.

(C–E) Energy level diagram of the (C) pristine, (D) ZnO-terminated, and (E) C-terminated LFP surface. For all samples, an image of the three highest occupied and three lowest unoccupied wave functions is shown. Within the energy diagrams, each line represents an orbital state where stronger colors show more orbital states with the same energy.

(F) Amplitude of the Li atom mean squared displacement (MSD) when the host lattice is fixed. The Li atoms are significantly more flexible close to the carbon termination with the other interfaces being relatively similar to Li-ion dynamics in the bulk of the lattice. Inset: Li ion trajectory of the pristine LFP sample when all atoms are allowed to move.

(amplitude of ~1.0 Å). With the distance between two interstitial Li hopping sites in LFP at ~1.8 Å,[45] the quasi-harmonic Li ion motion in the carbon terminated sample is already 60% of the hopping distance, compared to 40% for the pristine and ZnO terminated LFP surface. As a result, the energy needed from the host lattice to enable Li ion hopping in the carbon-coated LFP will be smaller. Increased Li-ion hopping between free lattice sites is indeed what we find from the AIMD simulations where all atoms are allowed to move (Figure S9). Within the slab, at the pristine surface, and with a ZnO termination, vibrations of the host lattice increase the MSD to 2.0 $Å^2$, 4.0 $Å^2$, and 3.0 $Å^2$, respectively. Meanwhile, in the carbon-terminated LFP, the vibrations of the host lattice increase the Li ion MSD one order of magnitude higher to 25 $Å^2$. This displacement enhancement is observed for all Li ions at the carbon-terminated surface (Figure S10).

Based on AIMD, we also distinguish between surface and interface diffusion. From the Li atom trajectories (inset Figures 3F and S7), we can infer that Li ions are mobile at the LFP interface along both the surface and interface diffusion directions. However, the effective distance traveled by the ions is different in the two cases. From the MSD (Figures S11 and S12), we find that, while interface and surface diffusion are very local in the ZnO and pristine-terminated LFP, the surface

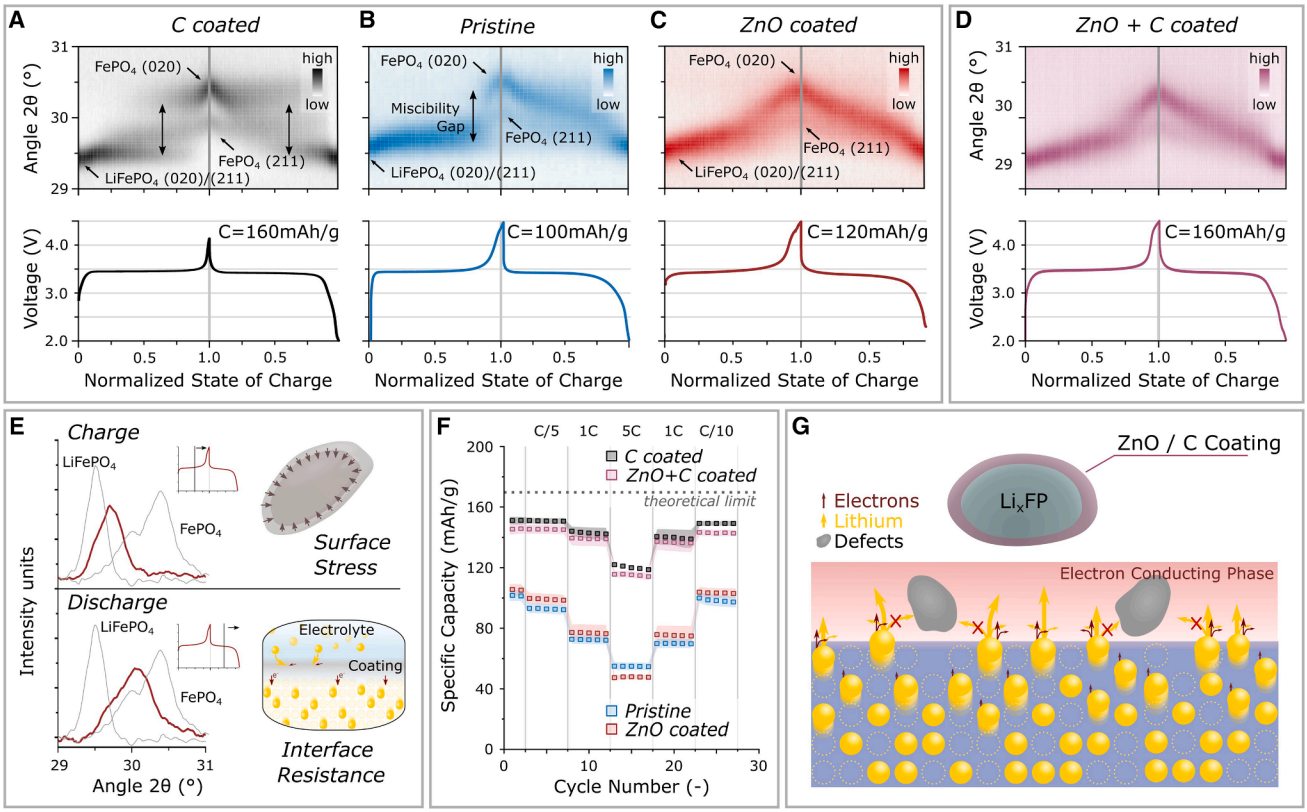

Figure 4. Studying (de)lithiation of $LiFePO_4$ *in situ* via X-ray diffraction

(A–D) Operando X-ray diffraction spectra of the $LiFePO_4$/$FePO_4$ (020) peak as a function of state of charge for (A) carbon-coated, (B) pristine, (C) ZnO-coated, and (D) ZnO + carbon-coated $LiFePO_4$ nanoparticles. All spectra were measured at a current of 17 mA/g corresponding to a rate of C/10.

(E) Comparison of the spectra at 50% (dis)charge at the ZnO sample. During particle charge, surface stress prevents phase separation. During discharge, the resistance due to the ZnO coating leads to a situation where charge transfer is faster than Li diffusion.

(F) Rate capability of the different coatings. Error bars represent the standard deviation of the capacity measured from three cells for each sample.

(G) Schematic of the hypothesis explaining the behavior of the ZnO+coating coating. Due to the ZnO defect regions, the surface diffusion of Li is impeded while the carbon matrix still allows for high rate capability and capacity retention.

diffusion dominates for the carbon-coated LFP. This effect persists even when the surface is lithium deficient (see Figure S13).

In summary, our experimental and computational findings on LFP particles with different coatings indicate that the carbon termination of LFP strongly enhances surface diffusion, which we attribute to the electronic structure difference at the LFP-coating interface, specifically the hybridization of Fe orbitals with carbon. This is further supported by a coordination bond that forms between iron and carbon (see Note S1).[47]

Consequences for the Li (de)intercalation

We expect that these differences in Li ion surface diffusion will influence the lithiation of the LFP samples. Specifically, we anticipate that ZnO and pristine coated $LiFePO_4$, with their relatively slow surface diffusion, will have a reduced critical current and favor lithiation via solid solution formation while carbon-coated $LiFePO_4$ will have an enhanced critical current and exhibit phase separation.

To check this, we perform *operando* X-ray diffraction (XRD) measurements on $LiFePO_4$ half cells (Figures 4A–4D). For reasons of the XRD data quality, the *operando* XRD spectra shown in Figure 4 are measured at a rate of 0.1C; however, measurements at a fast rate of 1C show the same charge-discharge behavior as at 0.1C (Figure S24). Focusing on the $LiFePO_4$/$FePO_4$ (020)/(211) peaks that are sensitive to the lithium ion distribution,[2,17] we see that the surface terminations indeed lead to different behavior during discharge (i.e., lithiation). In agreement with our expectations, only the carbon-coated sample (Figures 4A and S25) exhibits a miscibility gap indicative of phase separation. Meanwhile, the pristine (Figure 4B) and ZnO-coated (Figure 4C) $LiFePO_4$ particles demonstrate solid solution behavior (monotonous change in the XRD peak) and a curved voltage plateau (dQ/dV plot in Figure S26). A detailed calculation of the fraction between solid solution and phase separation, the so-called solid solution fraction (SSF),[20] supports our finding with an SSF of up to 80% for ZnO coating and only up to 50% for C coating (Figure S27). In addition, we confirm via *operando* XRD measurements on larger LFP particles of 300 nm diameter, that solid solution lithiation cannot solely be attributed to the relatively small particle size close to the characteristic phase boundary (Figure S28).

During charge (i.e., delithiation), we expect a miscibility gap in all samples due to the auto-catalytic nature of spinodal decomposition.[7,9,20] We indeed find a miscibility gap between $Li_{0.2}FePO_4$ and $Li_{0.8}FePO_4$ in the pristine and carbon-coated LFP samples. In the ZnO coated LFP sample, however, the miscibility gap is smaller, only appearing between $Li_{0.55}FePO_4$ and $Li_{0.7}FePO_4$.

Looking closer at the XRD pattern of the ZnO coating at a normalized state of charge of 50% (Figure 4E; other samples shown in Figure S30),[48–54] we observe an asymmetry between lithiation and delithiation. During discharge (lithiation), the (020) and (211) peaks broaden into each other as reported for solid solution lithation.[9] During charge (delithiation), the peaks only shift and lift the degeneracy without significant broadening, indicative of tensile stresses induced by the coating during delithiation.[55] We hypothesize that the impeded Li surface reorganization with the ZnO coating limits phase separation while adding tensile strain during delithiation (see Note S3), thereby reducing the miscibility gap.[56,57] The benefits of the ZnO coating thus appear to be 2-fold: it blocks Li surface diffusion forcing solid solution lithiation during discharge and also changes the mechanical properties at the surface, broadening the range of a $LiFePO_4$/$FePO_4$ solid solution during delithiation (charge).

While the reduction in phase separation for the case of the ZnO coating is promising, an underlying conflict exists. Figure 4F shows that a carbon coating, which facilitates electronic transfer to/from the carbon black network,[58] is crucial to extract the desired capacities above 150 mAh/g and achieve good rate capability. However, carbon-coating also enables fast Li surface diffusion, which leads to phase separation instead of the solid solution lithiation. In contrast, a non-electronically conductive coating (such as ZnO) that forces Li diffusion into the particle instead of along the LFP surface results in the desirable solid solution-based lithiation but exhibits poor capacity and rate capability.

Decoupling electronic and ionic transport

To facilitate solid solution lithiation and thus reduce inhomogeneous currents while at the same time achieving high capacities and rate capabilities, we propose a coating that promotes electron transfer while impeding the long-range surface diffusion of lithium. To test this hypothesis, we propose a carbon coating that contains ZnO regions and prepare ZnO/carbon-coated $LiFePO_4$ particles by mixing zinc acetate and D-glucose during the coating step (Figure S31). As sketched in Figure 4G, we expect the carbon part of the coating to offer good electronic transport and connection to the carbon-black network in the cathode, and, at the same time, we expect the ZnO clusters to impede long range lithium ion surface diffusion and to promote lithium ion transport through the coating into the particle (i.e., driving a solid solution). In addition, the ZnO clusters can lead to irregular electric field distributions in the coating that can trap the Li ions, further boosting the solid solution formation.

Our expectations are confirmed by *operando* XRD of the ZnO/carbon-coated $LiFePO_4$ (Figures 4D and S25), which reveals the same solid solution behavior as for the ZnO-coated $LiFePO_4$ (Figure 4C). Meanwhile, the measured electrochemical impedance profile (Figure S26) and the rate capability (Figure 4F) of the ZnO/carbon-coated $LiFePO_4$ is on par with that of carbon-coated $LiFePO_4$.

Conclusions

While optimization of the ZnO and C ratios and their distribution within the coating would likely offer additional possibilities to improve the material performance, this work highlights how surfaces can be used to control the (de)lithiation in battery active materials.

On one hand, our findings provide an explanation for the discrepancies in the reported LFP ion diffusivities. For example, Kang et al.[59] showed that a complex amorphous coating could lead to very high rate capabilities in LFP. Based on our findings, we hypothesize that the high diffusivity arises due to a hybridization of the Fe surface states that allows for enhanced charge dynamics. Also the inconsistency of measured LFP diffusivities using μ^+SR can be linked to surfaces, where solid state syntheses that are more prone to create amorphous interfaces,[31] typically lead to higher diffusivities[37,60] than solvothermal syntheses that typically form insulating hydroxide-terminated surfaces.[61,62]

At the same time, LFP with carbon coating is already an industrially relevant cathode material despite the phase separation due to its stable lattice.[2] The finding that phase separation can be effectively eliminated by creating coatings that impede Li surface transport but allow for fast ion transfer into the material can be transferred to other phase separating battery chemistries (e.g., Li air batteries,[63] transition metal oxides,[64] etc.) and materials where small polaron transport is the only available electron transfer path. Our findings also provide an explanation why the shift from phase separation to solid solution is only observed in materials with a low intrinsic electronic conductivity, such as Li_xFePO_4, but not in Li_xCoO_2 and Li_xC_6 ($0 < x < 1$).[65,66] As these materials have intrinsically high electronic conductivities, the Li reorganization via 2D diffusion in the bulk or at the surface is not constrained by electronic transport, favoring the thermodynamic equilibrium of phase separation.

Furthermore, our approach to study interface dynamics is transferable to other systems where interface dynamics has yet to be understood, e.g., solid electrolyte interphases[67,68] and solid state electrolyte interfaces.[69] Continuous developments of μ^+SR based on *in situ* setups,[70] muon focusing to interfaces,[71] and beamline upgrades will allow for increasing capabilities to measure surface dynamics in the near future. Combining this with novel modeling descriptions that include electronic contributions in the lithium ion diffusion process[72] might pave the way to understand charge transfer through complex systems, allowing new battery chemistries with higher rate capabilities, capacities, and longer battery life.

METHODS

Synthesis of coated $LiFePO_4$ nanoplatelets

We prepare $LiFePO_4$ samples in a modified solvothermal synthesis approach along the synthesis described before.[30] The coated $LiFePO_4$ nanoparticles with 3wt % ZnO and carbon are prepared by grinding $LiFePO_4$ particles together with zinc acetate (Sigma) or D-glucose (Sigma), respectively. The mixture is then pressed into pellets and annealed under Ar/3%H_2 flow. For the mixed

ZnO/carbon co-coated $LiFePO_4$ samples, zinc acetate and D-glucose are ground together with $LiFePO_4$ to achieve a mixture with 2.5 wt % ZnO, 2.5 wt % carbon, and 95 wt % $LiFePO_4$.

DFT simulations

We perform DFT calculations with the Quickstep module in the CP2k program suite.[39] The pristine and coated $LiFePO_4$ slabs are all geometrically relaxed. AIMD measurements are performed in the canonical ensemble at 1000 K.

μ^+SR measurements

μ^+SR measurements are performed on the EMU beamline at the ISIS Neutron and muon facility. Each $LiFePO_4$ sample (approx. 1.5 g) is pressed into pellets and sealed in a titanium sample holder with a 50-μm titanium window. The holder is mounted on a closed cycle refrigerator (CCR) for subsequent cooling to 50 K followed by heating in 12.5–50 K increments.

Electrochemical characterization

Electrochemical measurements are performed using half cells with metallic Li as counter electrode. For the $LiFePO_4$ nanoparticle electrodes, we prepare aqueous slurries that contain 85 wt % $LiFePO_4$, 10 wt % Super C65 carbon black (Timcal), and 5 wt % poly(acrylic acid) (Sigma, Mv ~450 000) at a solid content of approximately 20%. The slurry is blade casted on the Al current collector and dried in air. Before the cell assembly, the electrodes are then heated out at 80°C under vacuum for up to 12 h. The electrochemical characterizations are performed using the Biologic MPG2 potentiostat. For all galvanostatic measurements in $LiFePO_4$, the current at 1C rate was defined as 170 mA per gram of $LiFePO_4$.

Further information regarding the details of theoretical calculation, powder characterization and electrochemical measurement can be found in the supplemental information Section 1.

RESOURCE AVAILABILITY

Lead contact

For further information and resources, please contact the lead contact, Vanessa Claire Wood (vwood@ethz.ch).

Materials availability

All materials generated in this study are available from the lead contact upon reasonable request.

Data and code availability

The raw μ^+SR data are available under the data found at https://doi.org/10.5286/ISIS.E.RB1702326. All other experimental and computational data within the article and its supplemental information will be made available upon reasonable request to the lead contact.

ACKNOWLEDGMENTS

The authors acknowledge the Scientific Center for Optical and Electron Microscopy (ScopeM), the Swiss National Supercomputing Center (CSCS; project ID: s932). P.B., X.Z., and V.C.W. are supported by ERC Starting Grant (860070). R.S. was financially supported by the Swiss National Science Foundation (SNF) BRIDGE grant (40B1_0_184209). M. Medarde is supported from SNF R'equip grant no. 206021_138982. E.N. is fully financed by the Swedish Foundation for Strategic Research (SSF) within the Swedish National Graduate School in Neutron Scattering (SwedNess). P.B. and T.F.J. were supported by the U.S. Department of Energy, Office of Science, Office of Basic Energy Sciences, Chemical Sciences, Geosciences, and Biosciences Division, Catalysis Science Program through the SUNCAT Center for Interface Science and Catalysis.

AUTHOR CONTRIBUTIONS

P.B. and X.Z. conceived and designed the project, analyzed all experimental data, and performed the DFT simulations and electrochemical experiments. P.B., X.Z., and R.S. developed the electrode fabrication. E.R.B. and A.B. performed the X-ray photoemission spectroscopy measurements. P.B. and A.M. took EDS STEM images of the $LiFePO_4$ samples. P.B., O.K.F., N.M., E.N., Y.S., F.J., and M. Mansson measured the μ^+SR spectra and analyzed the data. S.C. prepared the EMU beamline for the μ^+SR measurements. M. Medarde performed the magnetic measurements. V.C.W. supervised the work. All authors contributed to writing the text. P.B. and X.Z. contributed equally to this study.

DECLARATION OF INTERESTS

The authors declare no competing interests.

SUPPLEMENTAL INFORMATION

Supplemental information can be found online at https://doi.org/10.1016/j.matt.2026.102725.

Received: October 20, 2025
Revised: February 10, 2026
Accepted: February 25, 2026
Published: March 27, 2026

REFERENCES

1. Chen, H., Benedek, P., Fisher, K.-J., Wood, V., and Cui, Y. (2020). Self-assembled materials for electrochemical energy storage. MRS Bull. *45*, 815–822. https://doi.org/10.1557/mrs.2020.247.
2. Lim, J., Li, Y., Alsem, D.H., So, H., Lee, S.C., Bai, P., Cogswell, D.A., Liu, X., Jin, N., Yu, Y.s., et al. (2016). Origin and hysteresis of lithium compositional spatiodynamics within battery primary particles. Science *353*, 566–571. https://doi.org/10.1126/science.aaf4914.
3. Zhang, W., Yu, H.-C., Wu, L., Liu, H., Abdellahi, A., Qiu, B., Bai, J., Orvananos, B., Strobridge, F.C., Zhou, X., et al. (2018). Localized concentration reversal of lithium during intercalation into nanoparticles. Sci. Adv. *4*, eaao2608. https://doi.org/10.1126/sciadv.aao2608.
4. Müller, S., Lippuner, M., Verezhak, M., De Andrade, V., De Carlo, F., and Wood, V. (2020). Multimodal nanoscale tomographic imaging for battery electrodes. Adv. Energy Mater. *10*, 1904119. https://doi.org/10.1002/aenm.201904119.
5. Shapiro, D.A., Yu, Y.-S., Tyliszczak, T., Cabana, J., Celestre, R., Chao, W., Kaznatcheev, K., Kilcoyne, A.L.D., Maia, F., Marchesini, S., et al. (2014). Chemical composition mapping with nanometre resolution by soft X-ray microscopy. Nat. Photonics *8*, 765–769. https://doi.org/10.1038/nphoton.2014.207.
6. Li, Y., El Gabaly, F., Ferguson, T.R., Smith, R.B., Bartelt, N.C., Sugar, J.D., Fenton, K.R., Cogswell, D.A., Kilcoyne, A.L.D., Tyliszczak, T., et al. (2014). Current-induced transition from particle-by-particle to concurrent intercalation in phase-separating battery electrodes. Nat. Mater. *13*, 1149–1156. https://doi.org/10.1038/nmat4084.
7. Bazant, M.Z. (2017). Thermodynamic stability of driven open systems and control of phase separation by electro-autocatalysis. Faraday Discuss. *199*, 423–463. https://doi.org/10.1039/C7FD00037E.
8. Malik, R., Zhou, F., and Ceder, G. (2011). Kinetics of non-equilibrium lithium incorporation in LiFePO4. Nat. Mater. *10*, 587–590. https://doi.org/10.1038/nmat3065.

9. Nadkarni, N., Rejovitsky, E., Fraggedakis, D., Di Leo, C.V., Smith, R.B., Bai, P., and Bazant, M.Z. (2018). Interplay of phase boundary anisotropy and electro-autocatalytic surface reactions on the lithium intercalation dynamics in LiXFePO4 platelet-like nanoparticles. Phys. Rev. Mater. *2*, 085406. https://doi.org/10.1103/PhysRevMaterials.2.085406.

10. Gabrisch, H., Wilcox, J., and Doeff, M.M. (2007). TEM studies of carbon coated LiFePO4 after charge discharge cycling. ECS Trans. *3*, 29–36. https://doi.org/10.1149/1.2795103.

11. Scipioni, R., Jørgensen, P.S., Hjelm, J., Norby, P., Rasmussen, C.N., and Jensen, S.H. (2015). Degradation studies on LiFePO4 cathode. ECS Trans. *64*, 97–104. https://doi.org/10.1149/06422.0097ecst.

12. Demirocak, D.E., and Bhushan, B. (2016). Probing the aging effects on nanomechanical properties of a thin film LiFePO4 cathode. ECS Trans. *73*, 57–66. https://doi.org/10.1149/07301.0057ecst.

13. Bai, P., Cogswell, D.A., and Bazant, M.Z. (2011). Suppression of phase separation in LiFePO4 nanoparticles during battery discharge. Nano Lett. *11*, 4890–4896. https://doi.org/10.1021/nl202764f.

14. Malik, R., Abdellahi, A., and Ceder, G. (2013). A critical review of the Li insertion mechanisms in LiFePO4 electrodes. J. Electrochem. Soc. *160*, A3179–A3197. https://doi.org/10.1149/2.029305jes.

15. Wagemaker, M., Mulder, F.M., and Van der Ven, A. (2009). The role of surface and interface energy on phase stability of nanosized insertion compounds. Adv. Mater. *21*, 2703–2709. https://doi.org/10.1002/adma.200803038.

16. Bazant, M.Z. (2013). Theory of chemical kinetics and charge transfer based on nonequilibrium thermodynamics. Acc. Chem. Res. *46*, 1144–1160. https://doi.org/10.1021/ar300145c.

17. Liu, H., Strobridge, F.C., Borkiewicz, O.J., Wiaderek, K.M., Chapman, K.W., Chupas, P.J., and Grey, C.P. (2014). Capturing metastable structures during high-rate cycling of LiFePO4 nanoparticle electrodes. Science *344*, 1252817. https://doi.org/10.1126/science.1252817.

18. Hess, M., Sasaki, T., Villevieille, C., and Novák, P. (2015). Combined operando X-ray diffraction–electrochemical impedance spectroscopy detecting solid solution reactions of LiFePO4 in batteries. Nat. Commun. *6*, 8169. https://doi.org/10.1038/ncomms9169.

19. Zhang, X., van Hulzen, M., Singh, D.P., Brownrigg, A., Wright, J.P., van Dijk, N.H., and Wagemaker, M. (2014). Rate-induced solubility and suppression of the first-order phase transition in olivine LiFePO4. Nano Lett. *14*, 2279–2285. https://doi.org/10.1021/nl404285y.

20. Li, Y., Chen, H., Lim, K., Deng, H.D., Lim, J., Fraggedakis, D., Attia, P.M., Lee, S.C., Jin, N., Moškon, J., et al. (2018). Fluid-enhanced surface diffusion controls intraparticle phase transformations. Nat. Mater. *17*, 915–922. https://doi.org/10.1038/s41563-018-0168-4.

21. Li, Y. (2018). A review of recent research on nonequilibrium solid solution behavior in LiXFePO4. Solid State Ion. *323*, 142–150. https://doi.org/10.1016/j.ssi.2018.05.026.

22. Zhang, X., Belharouak, I., Li, L., Lei, Y., Elam, J.W., Nie, A., Chen, X., Yassar, R.S., and Axelbaum, R.L. (2013). Structural and electrochemical study of Al2O3 and TiO2 coated Li1.2Ni0.13Mn0.54Co0.13O2 cathode material using ALD. Adv. Energy Mater. *3*, 1299–1307. https://doi.org/10.1002/aenm.201300269.

23. León, B., Vicente, C.P., Tirado, J.L., Biensan, P., and Tessier, C. (2008). Optimized chemical stability and electrochemical performance of LiFePO4 composite materials obtained by ZnO coating. J. Electrochem. Soc. *155*, A211–A216. https://doi.org/10.1149/1.2828039.

24. Doeff, M.M., Hu, Y., McLarnon, F., and Kostecki, R. (2003). Effect of surface carbon structure on the electrochemical performance of LiFePO4. Electrochem. Solid State Lett. *6*, A207–A209. https://doi.org/10.1149/1.1601372.

25. Morgan, D., Van der Ven, A., and Ceder, G. (2004). Li conductivity in LixMPO4 (M = Mn, Fe, Co, Ni) olivine materials. Electrochem. Solid State Lett. *7*, A30–A32. https://doi.org/10.1149/1.1633511.

26. Ellis, B., Perry, L.K., Ryan, D.H., and Nazar, L.F. (2006). Small polaron hopping in LixFePO4 solid solutions: Coupled lithium-ion and electron mobility. J. Am. Chem. Soc. *128*, 11416–11422. https://doi.org/10.1021/ja0614114.

27. Emin, D. (1975). Phonon-assisted transition rates I: Optical-phonon-assisted hopping in solids. Adv. Phys. X. *24*, 305–348. https://doi.org/10.1080/00018737500101411.

28. Dathar, G.K.P., Sheppard, D., Stevenson, K.J., and Henkelman, G. (2011). Calculations of Li-ion diffusion in olivine phosphates. Chem. Mater. *23*, 4032–4037. https://doi.org/10.1021/cm201604g.

29. Benedek, P., Yazdani, N., Chen, H., Wenzler, N., Juranyi, F., Månsson, M., Islam, M.S., and Wood, V.C. (2019). Surface phonons of lithium ion battery active materials. Sustain. Energy Fuels *3*, 508–513. https://doi.org/10.1039/C8SE00389K.

30. Benedek, P., Forslund, O.K., Nocerino, E., Yazdani, N., Matsubara, N., Sassa, Y., Jurànyi, F., Medarde, M., Telling, M., Månsson, M., and Wood, V. (2020). Quantifying diffusion through interfaces of lithium-ion battery active materials. ACS Appl. Mater. Interfaces *12*, 16243–16249. https://doi.org/10.1021/acsami.9b21470.

31. Wang, J., and Sun, X. (2012). Understanding and recent development of carbon coating on LiFePO4 cathode materials for lithium-ion batteries. Energy Environ. Sci. *5*, 5163–5185. https://doi.org/10.1039/C1EE01263K.

32. Cheng, J., Sivonxay, E., and Persson, K.A. (2020). Evaluation of amorphous oxide coatings for high-voltage Li-ion battery applications using a first-principles framework. ACS Appl. Mater. Interfaces *12*, 35748–35756. https://doi.org/10.1021/acsami.0c10000.

33. Benedek, P., Wenzler, N., Yarema, M., and Wood, V.C. (2017). Low temperature hydrothermal synthesis of battery grade lithium iron phosphate. RSC Adv. *7*, 17763–17767. https://doi.org/10.1039/C7RA00463J.

34. Dedryvère, R., Maccario, M., Croguennec, L., Le Cras, F., Delmas, C., and Gonbeau, D. (2008). X-ray photoelectron spectroscopy investigations of carbon-coated LixFePO4 materials. Chem. Mater. *20*, 7164–7170. https://doi.org/10.1021/cm801995p.

35. Sugiyama, J. (2019). Spin polarized beam for battery materials research: μ±SR and β-NMR. Hyperfine Interact. *240*, 17. https://doi.org/10.1007/s10751-019-1560-4.

36. Wilkening, M., Epp, V., Feldhoff, A., and Heitjans, P. (2008). Tuning the Li diffusivity of poor ionic conductors by mechanical treatment: High Li conductivity of strongly defective LiTaO3 nanoparticles. J. Phys. Chem. C *112*, 9291–9300. https://doi.org/10.1021/jp801537s.

37. Sugiyama, J., Nozaki, H., Harada, M., Kamazawa, K., Ofer, O., Månsson, M., Brewer, J.H., Ansaldo, E.J., Chow, K.H., Ikedo, Y., et al. (2011). Magnetic and diffusive nature of LiFePO4 investigated by muon spin rotation and relaxation. Phys. Rev. B *84*, 054430. https://doi.org/10.1103/PhysRevB.84.054430.

38. Hutter, J., Iannuzzi, M., Schiffmann, F., and VandeVondele, J. (2014). CP2K: Atomistic simulations of condensed matter systems. WIREs Comput. Mol. Sci. *4*, 15–25. https://doi.org/10.1002/wcms.1159.

39. VandeVondele, J., Krack, M., Mohamed, F., Parrinello, M., Chassaing, T., and Hutter, J. (2005). Quickstep: Fast and accurate density functional calculations using a mixed Gaussian and plane waves approach. Comput. Phys. Commun. *167*, 103–128. https://doi.org/10.1016/j.cpc.2004.12.014.

40. Perdew, J.P., Burke, K., and Ernzerhof, M. (1996). Generalized gradient approximation made simple. Phys. Rev. Lett. *77*, 3865–3868. https://doi.org/10.1103/PhysRevLett.77.3865.

41. Sumita, M., Tanaka, Y., Ikeda, M., and Ohno, T. (2015). Theoretically designed Li3PO4 (100)/LiFePO4 (010) coherent electrolyte/cathode interface for all solid-state Li ion secondary batteries. J. Phys. Chem. C *119*, 14–22. https://doi.org/10.1021/jp5060342.

42. Maxisch, T., Zhou, F., and Ceder, G. (2006). Ab initio study of the migration of small polarons in olivine LixFePO4 and their association with lithium ions

and vacancies. Phys. Rev. B *73*, 104301. https://doi.org/10.1103/PhysRevB.73.104301.

43. Wang, L., Zhou, F., Meng, Y.S., and Ceder, G. (2007). First-principles study of surface properties of LiFePO4: Surface energy, structure, Wulff shape, and surface redox potential. Phys. Rev. B *76*, 165435. https://doi.org/10.1103/PhysRevB.76.165435.
44. Park, K.-S., Xiao, P., Kim, S.-Y., Dylla, A., Choi, Y.-M., Henkelman, G., Stevenson, K.J., and Goodenough, J.B. (2012). Enhanced charge-transfer kinetics by anion surface modification of LiFePO4. Chem. Mater. *24*, 3212–3218. https://doi.org/10.1021/cm301569m.
45. Nishimura, S.i., Kobayashi, G., Ohoyama, K., Kanno, R., Yashima, M., and Yamada, A. (2008). Experimental visualization of lithium diffusion in LixFePO4. Nat. Mater. *7*, 707–711. https://doi.org/10.1038/nmat2251.
46. Kahle, L., Marcolongo, A., and Marzari, N. (2018). Modeling lithium-ion solid-state electrolytes with a pinball model. Phys. Rev. Mater. *2*, 065405. https://doi.org/10.1103/PhysRevMaterials.2.065405.
47. Poletayev, A.D., Dawson, J.A., Islam, M.S., and Lindenberg, A.M. (2022). Defect-driven anomalous transport in fast-ion conducting solid electrolytes. Nat. Mater. *21*, 1066–1073. https://doi.org/10.1038/s41563-022-01316-z.
48. Müller, S., Pietsch, P., Brandt, B.-E., Baade, P., De Andrade, V., De Carlo, F., and Wood, V. (2018). Quantification and modeling of mechanical degradation in lithium-ion batteries based on nanoscale imaging. Nat. Commun. *9*, 2340. https://doi.org/10.1038/s41467-018-04477-1.
49. Andersson, A., Kalska, B., Häggström, L., and Thomas, J.O. (2000). Lithium extraction/insertion in LiFePO4: An X-ray diffraction and Mössbauer spectroscopy study. Solid State Ion. *130*, 41–52. https://doi.org/10.1016/S0167-2738(00)00311-8.
50. García-Moreno, O., Alvarez-Vega, M., García-Jaca, J., García-Jaca, J., Sanjuán, M.L., Sanjuán, M.L., and Amador, U. (2001). Influence of the structure on the electrochemical performance of lithium transition metal phosphates as cathodic materials in rechargeable lithium batteries: A new high-pressure form of LiMPO4 (M = Fe and Ni). Chem. Mater. *13*, 1570–1576. https://doi.org/10.1021/cm000596p.
51. Onoprienko, A.A., and Yanchuk, I.B. (2006). Temperature dependence of the mechanical properties of amorphous carbon films deposited by magnetron sputtering. Powder Metall. Met. Ceram. *45*, 190–195. https://doi.org/10.1007/s11106-006-0062-5.
52. Arai, Y., Daigo, Y., Kojo, E., Inoue, R., and Kogo, Y. (2021). Relationship between the microstructures and Young's modulus of 3D-networked porous carbon material. J. Mater. Sci. *56*, 10338–10352. https://doi.org/10.1007/s10853-021-05950-x.
53. Wang, M., and Ye, H. (2022). Microstructure dependent chemo-mechanical behavior of amorphous Si anodes for Li-ion batteries upon delithiation. J. Power Sources *520*, 230803. https://doi.org/10.1016/j.jpowsour.2021.230803.
54. Dong, H., Guo, H., He, Y., Gao, J., Han, W., Lu, X., Yan, S., Yang, K., Li, H., Chen, D., and Li, H. (2017). Structural stability and Li-ion transport property of LiFePO4 under high pressure. Solid State Ion. *301*, 133–137. https://doi.org/10.1016/j.ssi.2017.01.026.
55. Cortes, F.J.Q., Boebinger, M.G., Xu, M., Ulvestad, A., and McDowell, M.T. (2018). Operando synchrotron measurement of strain evolution in individual alloying anode particles within lithium batteries. ACS Energy Lett. *3*, 349–355. https://doi.org/10.1021/acsenergylett.7b01185.
56. Meethong, N., Huang, H.-Y.S., Carter, W.C., and Chiang, Y.-M. (2007). Size-dependent lithium miscibility gap in nanoscale Li1−xFePO4. Electrochem. Solid State Lett. *10*, A134–A138. https://doi.org/10.1149/1.2710960.
57. Cogswell, D.A., and Bazant, M.Z. (2012). Coherency strain and the kinetics of phase separation in LiFePO4 nanoparticles. ACS Nano *6*, 2215–2225. https://doi.org/10.1021/nn204177u.
58. Huang, H., Yin, S.-C., and Nazar, L.F. (2001). Approaching theoretical capacity of LiFePO4 at room temperature at high rates. Electrochem. Solid State Lett. *4*, A170–A172. https://doi.org/10.1149/1.1396695.
59. Kang, B., and Ceder, G. (2009). Battery materials for ultrafast charging and discharging. Nature *458*, 190–193. https://doi.org/10.1038/nature07853.
60. Baker, P.J., Franke, I., Pratt, F.L., Lancaster, T., Prabhakaran, D., Hayes, W., and Blundell, S.J. (2011). Probing magnetic order in LiMPO4 (M = Ni, Co, Fe) and lithium diffusion in LixFePO4. Phys. Rev. B *84*, 174403. https://doi.org/10.1103/PhysRevB.84.174403.
61. Ashton, T.E., Laveda, J.V., MacLaren, D.A., Baker, P.J., Porch, A., Jones, M.O., and Corr, S.A. (2014). Muon studies of Li+ diffusion in LiFePO4 nanoparticles of different polymorphs. J. Mater. Chem. A *2*, 6238–6245. https://doi.org/10.1039/C4TA00543K.
62. Johnson, I.D., Ashton, T.E., Blagovidova, E., Smales, G.J., Lübke, M., Baker, P.J., Corr, S.A., and Darr, J.A. (2018). Mechanistic insights of Li+ diffusion within doped LiFePO4 from muon spectroscopy. Sci. Rep. *8*, 4114. https://doi.org/10.1038/s41598-018-22435-1.
63. Horstmann, B., Gallant, B., Mitchell, R., Bessler, W.G., Shao-Horn, Y., and Bazant, M.Z. (2013). Rate-dependent morphology of Li2O2 growth in Li–O2 batteries. J. Phys. Chem. Lett. *4*, 4217–4222. https://doi.org/10.1021/jz401973c.
64. Park, J., Zhao, H., Kang, S.D., Lim, K., Chen, C.-C., Yu, Y.-S., Braatz, R.D., Shapiro, D.A., Hong, J., Toney, M.F., et al. (2021). Fictitious phase separation in Li layered oxides driven by electro-autocatalysis. Nat. Mater. *20*, 991–999. https://doi.org/10.1038/s41563-021-00936-1.
65. Fraggedakis, D., Nadkarni, N., Gao, T., Zhou, T., Zhang, Y., Han, Y., Stephens, R.M., Shao-Horn, Y., and Bazant, M.Z. (2020). A scaling law to determine phase morphologies during ion intercalation. Energy Environ. Sci. *13*, 2142–2152. https://doi.org/10.1039/D0EE00653J.
66. Merryweather, A.J., Schnedermann, C., Jacquet, Q., Grey, C.P., and Rao, A. (2021). Operando optical tracking of single-particle ion dynamics in batteries. Nature *594*, 522–528. https://doi.org/10.1038/s41586-021-03584-2.
67. Shadike, Z., Lee, H., Borodin, O., Cao, X., Fan, X., Wang, X., Lin, R., Bak, S.-M., Ghose, S., Xu, K., et al. (2021). Identification of LiH and nanocrystalline LiF in the solid–electrolyte interphase of lithium metal anodes. Nat. Nanotechnol. *16*, 549–554. https://doi.org/10.1038/s41565-020-00845-5.
68. Liu, J., Bao, Z., Cui, Y., Dufek, E.J., Goodenough, J.B., Khalifah, P., Li, Q., Liaw, B.Y., Liu, P., Manthiram, A., et al. (2019). Pathways for practical high-energy long-cycling lithium metal batteries. Nat. Energy *4*, 180–186. https://doi.org/10.1038/s41560-019-0338-x.
69. Banerjee, A., Wang, X., Fang, C., Wu, E.A., and Meng, Y.S. (2020). Interfaces and interphases in all-solid-state batteries with inorganic solid electrolytes. Chem. Rev. *120*, 6878–6933. https://doi.org/10.1021/acs.chemrev.0c00101.
70. McClelland, I., Booth, S.G., El-Shinawi, H., Johnston, B.I.J., Clough, J., Guo, W., Cussen, E.J., Baker, P.J., and Corr, S.A. (2021). In situ diffusion measurements of a NASICON-structured all-solid-state battery using muon spin relaxation. ACS Appl. Energy Mater. *4*, 1527–1536. https://doi.org/10.1021/acsaem.0c02722.
71. Woerle, J., Prokscha, T., and Grossner, U. (2020). Low-energy muons as a tool for a depth-resolved analysis of the SiO2/4H-SiC interface. Mater. Sci. Forum *1004*, 581–586. https://doi.org/10.4028/www.scientific.net/MSF.1004.581.
72. Fraggedakis, D., McEldrew, M., Smith, R.B., Krishnan, Y., Zhang, Y., Bai, P., Chueh, W.C., Shao-Horn, Y., and Bazant, M.Z. (2021). Theory of coupled ion-electron transfer kinetics. Electrochim. Acta *367*, 137432. https://doi.org/10.1016/j.electacta.2020.137432.